inorganics

MDPI

Article

Calcium-Based Sorbent Carbonation at Low Temperature via Reactive Milling under CO_2

Seyed Morteza Taghavi Kouzehkanan [1], Ehsan Hassani [2], Farshad Feyzbar-Khalkhali-Nejad [1] and Tae-Sik Oh [1,*]

[1] Department of Chemical Engineering, Auburn University, Auburn, AL 36849, USA; szt0077@auburn.edu (S.M.T.K.); fzf0004@auburn.edu (F.F.-K.-N.)
[2] Manufacturing Excellence Division, International Paper, Prattville, AL 36067, USA; ehsan.hassani@ipaper.com
* Correspondence: taesik.oh@auburn.edu

Abstract: The carbonation behavior of calcium-containing sorbents, CaO and $Ca(OH)_2$, was investigated under pressurized CO_2 at nominal room temperature. The carbonation reaction was mechanically driven via reactive ball milling. The carbonation rate was determined by monitoring the CO_2 pressure inside the sealed milling jar. Two different versions of CaO were fabricated as starting materials. The addition of citric acid in CaO synthesis resulted in a significant increase in sorbent surface area, bringing up the conversion of CO_2 from 18% to 41% after 3 h of reactive milling. The hydroxide formation from these two oxides closed the surface area gap. Nevertheless, we found that hydroxides had a higher initial carbonation rate and greater final CO_2 uptake than their oxide counterparts. However, the formation of byproduct water limited the further carbonation of $Ca(OH)_2$. When we added a controlled amount of water to the CaO-containing milling jar, the highest carbonation rate and most extensive CO_2 uptake were attained due to the in situ formation of reactive $Ca(OH)_2$ nanoparticles. We saw $CaCO_3$ X-ray diffraction peaks only when $Ca(OH)_2$ was involved in this low-temperature carbonation, indicating that the grain growth of $CaCO_3$ is easier on the $Ca(OH)_2$ surface than on the CaO surface. We used the Friedman isoconversional method to calculate the effective activation energy of decarbonation for the high surface area CaO sorbent milled with water. The average effective activation energy was found to be about 72 kJ mol^{-1}, and its magnitude started to decrease significantly from 50% sorbent regeneration. The drastic change of the effective activation energy during decarbonation suggests that $CaCO_3$, formed at nominal room temperature by reactive milling under pressurized CO_2, should undergo a more drastic morphology change than the typical thermally carbonated $CaCO_3$.

Keywords: carbonation; decarbonation; reactive milling; mechanochemistry

Citation: Taghavi Kouzehkanan, S.M.; Hassani, E.; Feyzbar-Khalkhali-Nejad, F.; Oh, T.-S. Calcium-Based Sorbent Carbonation at Low Temperature via Reactive Milling under CO_2. *Inorganics* **2023**, *11*, 200. https://doi.org/10.3390/inorganics11050200

Academic Editor: Maurizio Peruzzini

Received: 30 March 2023
Revised: 25 April 2023
Accepted: 30 April 2023
Published: 3 May 2023

1. Introduction

CO_2 capture and storage will play a significant role in climate change mitigation. In addition to industrialized amine-based media, CaO and $Ca(OH)_2$ have been extensively studied as promising CO_2 capture media due to their ability to form calcium carbonate [1–5]. They are especially suited for the post-combustion carbon capture process since they can be applied to existing thermal power plants without significant equipment changes [6–8]. In this scheme, differing from the direct air capture, we have a high concentration of CO_2 in the flue gas and an elevated temperature. The $CaO/Ca(OH)_2$ carbonation typically occurs in the temperature window ranging from 600 to 750 °C [9–12]. This elevated temperature is needed to ensure a high enough carbonation reaction rate; however, it also unavoidably promotes the sintering of the sorbent. The sintering of the sorbent is a well-known persistent problem of the calcium-based solid sorbent since it leads to a loss of the solid sorbent surface area and a loss of the CO_2 capture capacity [13–16].

Many efforts have aimed to minimize the sintering of the calcium-based sorbent. The addition of inert oxide as a sintering barrier is a common practice [13,17]. The inert oxide

particles do not undergo a carbonation reaction and interrupt the sintering. In many cases, the addition of the inert oxides resulted in the formation of calcium-containing ternary oxides, such as $Ca_{12}Al_{14}O_{33}$ [16–19]. The beneficial impact of $CaZrO_3$ island formation for the CaO-ZrO_2 composite sorbent has been demonstrated, showing enhanced carbonation-decarbonation cycle stability [11,20–22].

Another approach is the modification of the sorbent morphology. Multishelled hollow microspheres of CaO have been synthesized with MgO stabilizer through a hydrothermal fabrication route [23]. Their CO_2 uptake was about 5 times higher than the limestone-derived CaO after 30 cycles of carbonation at 650 °C and decarbonation at 900 °C. Coating the CaO sorbent layer on an existing backbone material was proposed as a simple and effective way to control the CaO microstructure. When CaO was coated on the surface of Saffil ceramic fiber by wet impregnation, there was a trade-off between the cycle stability and initial CO_2 capture capacity since the higher loading of CaO led to more severe degradation [24]. Electrospinning and templating strategies have been adopted. Electrospinning makes it possible to control the diameter of the as-spun fiber before polymer burn-off. Even though the fibrous structure collapses after polymer removal, the fiber-derived CaO sorbent has shown a high initial CO_2 capture capacity compared to the CaO sorbent from a hydrothermal route [25]. The aluminum doping was effective for the fiber-derived CaO sorbent, greatly enhancing the cycle stability by forming $Ca_{12}Al_{14}O_{33}$ spacer particles at the expense of a small decrease in the initial CO_2 capacity [25]. For sacrificial templates, polystyrene microspheres [26], carbon spheres [27], paper fibers [28], carbon nanotubes [29], soft wood [2], and cotton fibers [29] have been used to render a porous structure in the solid sorbent.

Our group recently reported the impact of mechanical activation on the $Ca(OH)_2$ sorbent for post-combustion CO_2 capture [9]. The effect of the structural modification persisted over 10 cycles, leading to higher reaction rates in both carbonation and decarbonation steps compared to the untreated case. Especially, in situ X-ray diffraction results indicated that the mechanically activated samples had large (~110 nm) residual CaO crystallites after 20 min of carbonation at 700 °C. It was speculated that they facilitated the decarbonation of $CaCO_3$ by scavenging small newly forming CaO particles [9].

Taking one step further, we hereby study the mechanically driven carbonation of calcium-containing sorbents at nominal room temperature. Citric acid was used to control the initial CaO sorbent surface area. Most CO_2 mineralization studies conducted at low temperatures (<200 °C) investigated waste materials, including coal fly-ash [30,31], or naturally occurring sorbents, such as Olivine (Mg_2SiO_4) and Wollastonite ($CaSiO_3$) [32]. In this study, CaO, $Ca(OH)_2$, and water are the only chemicals other than CO_2. Zirconia milling balls were used to drive the carbonation reaction and reduce the average particle size of the calcium-based sorbent and calcium carbonate product. A similar reactive ball milling approach can be found for Mg-based hydrogen storage, where magnesium reacts with hydrogen to form MgH_2 [33].

2. Experimental

2.1. Sorbent Preparation

2.1.1. CaO Preparation

Calcium oxide was made from calcium nitrate tetrahydrate ($Ca(NO_3)_2{\cdot}4H_2O$) obtained from BeanTown Chemical (Hudson, NH, USA) with a purity of 99%, through two distinct methods. The first method involved heating the nitrate source in an oven at a temperature of 900 °C for a period of 2 h, with a heating rate of 10 °C/min, starting from the room temperature. To confirm the successful formation of CaO, X-ray diffraction testing was performed on the resulting sample using a Proto manufacturing AXRD powder diffraction system with Cu K_α radiation (λ = 1.5418 Å). This sample was subsequently named CaO-N. The second method involved dissolving calcium nitrate tetrahydrate and citric acid in a 1:1 molar ratio in 40 mL of deionized water, and stirring the solution at room temperature for 2 h. Subsequently, the solution was heated to evaporate water. A gel was formed, and the

gel underwent combustion and transformed into ash as the temperature increased. The ash was then placed in an oven and calcined at 900 °C for 2 h, with the same temperature ramp rate for CaO-N. The resulting sample was named CaO-NC.

2.1.2. $Ca(OH)_2$ Preparation

To synthesize $Ca(OH)_2$ sorbents, the previously prepared CaO-N and CaO-NC samples were subjected to a tube furnace process. During this process, the powder sample was exposed to a humidified nitrogen flow (3 vol% H_2O, 100 sccm) for 8 h at 140 °C. The powder sample was placed in a ceramic boat residing at the center of a horizontal quartz tube (diameter 25 mm). The resulting samples were confirmed to be $Ca(OH)_2$ through X-ray diffraction analysis. Based on their CaO sources, these samples were named $Ca(OH)_2$-N and $Ca(OH)_2$-NC, respectively.

To understand the physical properties of all the sorbents, nitrogen adsorption and desorption isotherms were measured using a Quantachrome NOVA 2200e instrument (Quantachrome, Boynton Beach, FL, USA). The surface area and pore volume were calculated using the Brunner−Emmett−Teller (BET) method based on nitrogen physisorption results. Additionally, the pore diameter distribution was calculated using the Barrett–Joyner–Hanelda (BJH) method.

2.2. Reactive Milling Carbonation

We investigated the reactive milling carbonation behaviors of calcium-based sorbents using a 200 mL stainless steel jar (height: 112 mm, inner diameter: 50 mm, outer diameter: 75 mm). We specifically designed a stainless steel lid to enable the reactive milling process. A hole was drilled through the lid and sealed off by a 5.5 mm diameter septa (Thermolite, Restek, Bellefonte, PA, USA) at the center of the hole. The gap between the septa and the hole wall was sealed using J-B Weld glue. Another hole was made similarly. When poked through by needles, the two septas provided one inlet and one outlet, forming a continuous gas pathway throughout the milling jar. For reactive milling carbonation, 250 g of 3 mm zirconia balls were first introduced to fill 50 mL of the milling jar volume from the bottom. After feeding either $Ca(OH)_2$ or CaO in the jar, we filled the jar with pure CO_2 to a pressure of 34.8 psia. We did not go to higher pressures for the safe operation of the milling jar. The CO_2 leakage was undetectable with this initial CO_2 pressure. We injected CO_2 through a 0.7 mm diameter needle, pushing out the initial air through another needle. To ensure that the jar was filled with CO_2 without any remaining air, the CO_2 flow was on for 10 min before cutting off the outlet flow by pulling out the downstream needle from the downstream septa. With the closed outlet, we adjusted the initial CO_2 pressure. The stoichiometric amount of sorbents to consume 34.8 psia of CO_2 was calculated. The calculated amount for $Ca(OH)_2$ was 1.1 g. However, considering the sorbent's available surface area and reaction sites, a decision was made to feed more sorbent than the exact stoichiometric requirement. Consequently, 3 g of $Ca(OH)_2$ sorbent and 2.27 g of CaO sorbent were used. The number of moles for calcium was kept the same in both cases.

Finally, the jar was placed in a planetary ball mill (PQ-N2 Across International) and ran at a speed of 300 rpm. Additionally, in some runs, a controlled amount of water was added to the calcium oxide for the reactive milling carbonation. To completely convert 2.27 g of CaO to $Ca(OH)_2$, 0.73 g of H_2O is required. To ensure in situ hydroxide formation during milling, three times the required amount was added to the jar: 2.19 g H_2O and 2.27 g CaO. The in situ formed $Ca(OH)_2$ is expected to have high carbonation reactivity due to its small size.

The CO_2 pressure in the jar was monitored over time using a Heise ST-2H bench top digital pressure indicator. We stopped the planetary mill to take the pressure measurements. After reading the pressure, reactive milling resumed immediately. The conversion of CO_2 was calculated using the following equation:

$$CO_2\ conversion\ (\%) = \frac{p_0 - p}{p_0} \times 100 \quad (1)$$

where p_0 is the initial pressure of CO_2 and p is the pressure of CO_2 during carbonation.

After the mechanically driven carbonation, the samples were collected to take X-ray diffraction patterns. Some samples were selected to carry out temperature-programmed decarbonation tests.

2.3. Temperature-Programmed Decarbonation

Temperature-programmed decarbonation experiments were conducted using 0.05 g of the ball-milled samples, which were loaded in a ceramic boat and then put in a quartz tube which was then placed in a tube furnace. Decarbonation tests were conducted under 100 sccm air flow by raising the spent sorbent temperature from the room temperature to 1050 °C, with four different temperature ramp rates: 2.5 °C/min, 5 °C/min, 10 °C/min, and 15 °C/min. The air flow rate was controlled by the mass flow controller, and the CO_2 concentration in the exhaust gas was monitored by a CO_2 sensor (ExplorIR®-M CO_2 Sensor, CM-40831, Thief River Falls, MN, USA).

We used this data to calculate the activation energy as a kinetic parameter based on the Friedman isoconversional method, which is the most common differential isoconversional method [34]. In general, the kinetic methods used under the constant heating rate for thermal analysis assume that the rate of the reaction is a function of conversion and temperature.

$$\frac{d\alpha}{dt} = k(T)f(\alpha) \tag{2}$$

k(T) is the chemical reaction rate constant (min^{-1}), α is the extent of conversion, and *f(α)* is the reaction model. Experimental measurements are used to determine the extent of conversion, which represents the fraction of the overall released CO_2 from $CaCO_3$, observed at different times or temperatures. α increases from 0 at the initiation of the reaction and reaches 1 when the reaction completes. The magnitude of α indicates the progress of the decarbonation of the sorbent. We can use Equation (3) to calculate α at different times.

$$\alpha = \frac{\int_0^t C_{CO_2} dt}{\int_0^{t_f} C_{CO_2} dt} \tag{3}$$

where t_f is the final time when CO_2 release is completed ($0 < t < t_f$).

The rate constant *k(T)* can be described by the Arrhenius equation [35]:

$$k(T) = A \exp\left(\frac{-E_a}{RT}\right) \tag{4}$$

where A is the frequency factor (min^{-1}), E_a is the activation energy (J/mol), R is the gas constant (8.314 J mol^{-1} K^{-1}), and T is the temperature (K).

So, by combining Equations (2) and (4), we have:

$$\frac{d\alpha}{dt} = A \exp\left(\frac{-E_a}{RT}\right) f(\alpha). \tag{5}$$

For a nonisothermal program in which the temperature changes linearly with time, the heating rate β (K/min) is constant and can be described as follows:

$$\beta = \frac{dT}{dt}. \tag{6}$$

Applying Equation (6) into Equation (5) results in:

$$\beta \frac{d\alpha}{dT} = A \exp\left(\frac{-E_a}{RT}\right) f(\alpha). \tag{7}$$

The equation for the Friedman isoconversional method is obtained from Equation (5) [34–36]:

$$\ln\left(\frac{d\alpha}{dt}\right)_{\alpha,i} = \ln(f(\alpha)A_\alpha) - \frac{E_\alpha}{RT_{\alpha,i}}. \quad (8)$$

The index "*i*" identifies different heating rate programs. Under the "*i*th" temperature program, the temperature at which the extent of conversion α is reached is denoted as $T_{\alpha,i}$. For each given conversion fraction α, by plotting the $ln\left(\frac{d\alpha}{dt}\right)_{\alpha,i}$ versus $\frac{1}{T_{\alpha,i}}$ at different heating rates, the slope of the line gives us the activation energy E_α.

For a nonisothermal process with a constant heating rate β, Equation (8) could also be written as [34]:

$$\ln[\beta_i\left(\frac{d\alpha}{dT}\right)_{\alpha,i}] = \ln(f(\alpha)A_\alpha) - \frac{E_\alpha}{RT_{\alpha,i}} \quad (9)$$

3. Results and Discussion

3.1. Sorbent Characterization

Figure 1 shows the X-ray diffraction patterns of as-synthesized CaO and $Ca(OH)_2$ sorbents. CaO-N, the oxide sorbent made without citric acid, was converted to $Ca(OH)_2$-N via the reaction with humid nitrogen at 140 °C. "-N" in the sample naming denotes the calcium nitrate precursor. The same process converted CaO-NC, the sorbent made with citric acid, to $Ca(OH)_2$-NC. "-NC" in the sample naming denotes the calcium source and citric acid. The 8 h reaction time was necessary to achieve the complete elimination of the remaining X-ray diffraction peaks from CaO. The citric acid addition in the CaO preparation step did not result in any significant microstructural difference in the $Ca(OH)_2$ sorbents probed by X-ray diffraction.

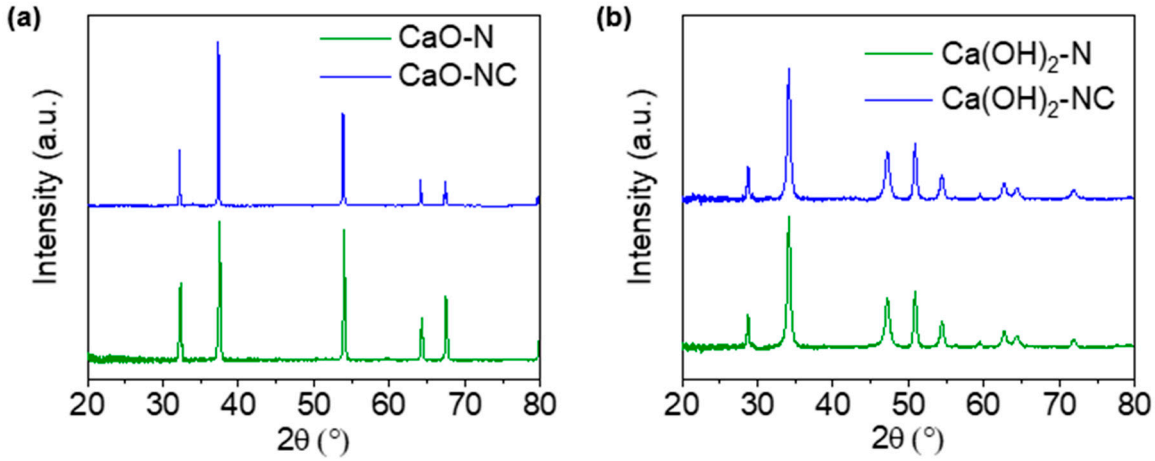

Figure 1. XRD patterns of (**a**) CaO sorbents prepared with or without citric acid and (**b**) $Ca(OH)_2$ sorbents prepared with or without citric acid.

All the sorbents were characterized for their pore structures and surface areas by nitrogen physisorption. The results are summarized in Table 1. Pore size distributions and nitrogen adsorption isotherms can be found in the supplementary materials (Figures S1 and S2). When we used citric acid in CaO sorbent synthesis, the sorbent BET surface area increased significantly; however, this surface area difference diminished after the conversion of CaO to $Ca(OH)_2$. Hydroxide formation increased the surface area of the low surface area sorbent (from 14.7 to 29.1 m^2/g) while lowering the surface area of the high surface area sorbent (from 50.9 to 34.1 m^2/g). Eventually, $Ca(OH)_2$-NC still had a higher surface area than $Ca(OH)_2$-N under the tested hydroxide formation condition. If the hydroxide grain growth was carried out over a longer period of time (>8 h), we would have an even more similar

surface area and pore size distribution regardless of the citric acid usage in the initial CaO preparation.

Table 1. Structural properties of the prepared sorbents.

Sorbent Name	BET Surface Area (m^2/g)	Total Pore Volume (cm^3/g)	Average Pore Diameter (nm)
CaO-N	14.7	0.015	4.20
$Ca(OH)_2$-N	29.1	0.149	10.3
CaO-NC	50.9	0.099	7.76
$Ca(OH)_2$-NC	34.1	0.135	7.9

3.2. Sorbent Carbonation by Reactive Milling

Figure 2 shows the CO_2 consumption over time and corresponding CO_2 conversion of the sorbents made without citric acid. The CO_2 pressure in the milling jar was measured every 30 min for 3 h. The carbonation rate of $Ca(OH)_2$-N exceeds that of CaO-N, as expected. It is well documented that $Ca(OH)_2$ carbonation is easier than CaO carbonation in the post-combustion CO_2 capture literatures. The inevitable formation of byproduct liquid water during hydroxide carbonation does not interfere with the carbonation reaction, reaching around 80% CO_2 conversion in 3 h. The most interesting result from Figure 2 is the very rapid consumption of CO_2 when water is added to CaO-N in the milling jar. Its carbonation rate was the highest of the three cases. The in situ formation of $Ca(OH)_2$ on the CaO particle surface may have taken place during reactive milling. The presumably nanograined $Ca(OH)_2$ can react with CO_2 rapidly, leading to the observed enhancement of carbonation kinetics. Even with the enhanced carbonation, 3.7 psia of CO_2 remained after 3 h of milling. The mechanical milling was not able to drive carbonation further. All CO_2 consumption took place within the initial 30 min.

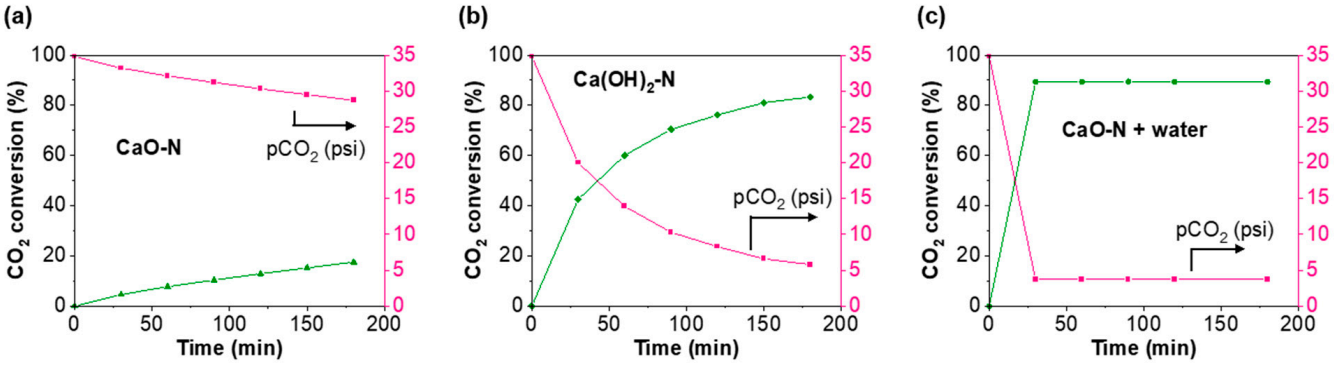

Figure 2. Conversion of CO_2 over time for different sorbents made without citric acid. (**a**) CaO-N, (**b**) $Ca(OH)_2$- N, and (**c**) CaO-N with added water. Conditions: initial CO_2 pressure: 34.8 psia, ball milling speed: 300 rpm.

Similar carbonation tests were conducted for the sorbents fabricated with citric acid. The as-synthesized sorbent should have a preferable pore structure for carbonation. Figure 3a shows the improvement of the carbonation kinetics. After 3 h of reactive milling, the CO_2 conversion for CaO-NC is more than double that of CaO-N. The favored pore structure induced by citric acid templating persisted after even hydroxide formation, as manifested by the rapid carbonation of $Ca(OH)_2$-NC (Figure 3b). However, after the fast initial carbonation of $Ca(OH)_2$-NC, the CO_2 conversion showed an unexpected plateau at 66%. It is clear that the limited carbonation originated from a kinetical barrier, since higher CO_2 conversion was possible (Figure 2b). The only reasonable explanation would be the formation of dense calcium carbonate shells that completely cover the surface of calcium hydroxide particles, even under continuous milling. The wet agglomeration of the $Ca(OH)_2$-$CaCO_3$ composite may proceed due to the presence of water generated by

hydroxide carbonation. The mechanical strength of the agglomerated composite particle and its relative size with respect to the milling balls (3 mm diameter) will determine the fracture probability. Fracturing clearly did not take place, prohibiting fresh $Ca(OH)_2$ surface exposure to CO_2. Therefore, further CO_2 capture is not possible. The initial carbonation rate (water formation rate) determines the emergence of the dense carbonate shell that does not break easily. The addition of water to CaO-NC, as expected, induced rapid CO_2 capture. When water is added to CaO for the reactive milling carbonation, the citric acid templating did not significantly impact the carbonation rate and final CO_2 conversion.

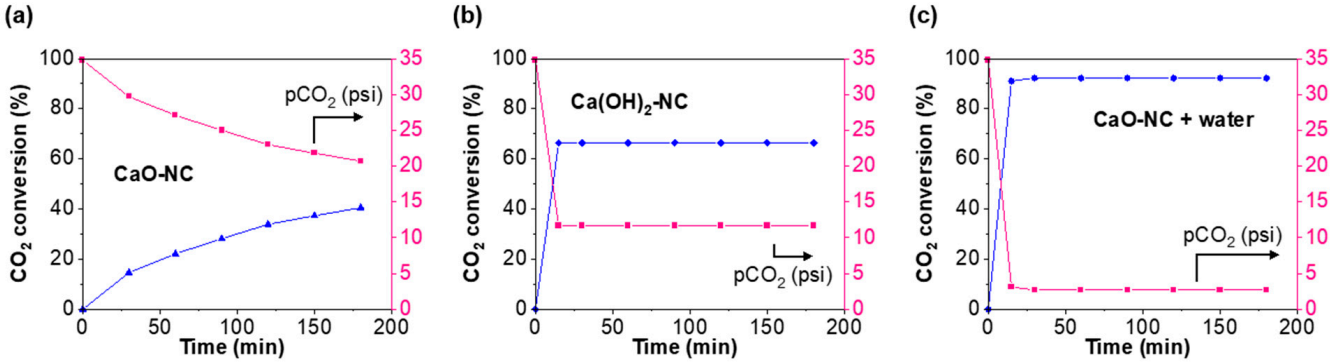

Figure 3. Conversion of CO_2 over time for different sorbents made with citric acid. (**a**) CaO-NC, (**b**) $Ca(OH)_2$- NC, and (**c**) CaO-NC with added water. The first data point is collected at 20 min mark. Conditions: initial CO_2 pressure: 34.8 psia, ball milling speed: 300 rpm.

After reactive milling carbonation, we collected the X-ray diffraction patterns of the spent sorbents. Figure 4 compares all the spent sorbents. For CaO-N and CaO-NC, only CaO diffraction peaks were observed, even though it is clear that $CaCO_3$ should have formed, considering the consumption level of CO_2. The low carbonation temperature led to either the formation of amorphous $CaCO_3$ or very small crystallites of $CaCO_3$, so we could not detect $CaCO_3$ diffraction peaks. The exact temperature of the instantaneous hot spots during reactive milling is difficult to measure. For $Ca(OH)_2$-N and $Ca(OH)_2$-NC, there is no significant difference between the diffraction patterns, even though the temporal CO_2 pressure evolution differs greatly. The water-added cases shared similar diffraction patterns. When $Ca(OH)_2$ participated in the carbonation reaction, the $CaCO_3$ product showed clear diffraction peaks, indicating that the grain growth of $CaCO_3$ is easier on the $Ca(OH)_2$ surface than on the CaO surface. In situ generated $Ca(OH)_2$ particles provided active sites for carbonation.

3.3. Spent Sorbent Regeneration

We further investigated the decarbonation behavior of the CaO sorbents milled with water under pressurized CO_2 by temperature-programmed decarbonation in air (10 °C/min ramp rate). The solid sorbent regeneration profiles had a common shape. The regeneration of the CaO-NC sorbent milled with water was relatively sluggish compared to the CaO-N sorbent milled with water, but not by much (Figure 5). The observed decarbonation behavior agrees well with the similarities found in the carbonation rates under reactive milling and post-reaction X-ray diffraction patterns.

The decarbonation behavior of the CaO-NC sorbent milled with water was further analyzed using the Friedman method with four different temperature ramp rates. These ramp rates were chosen for a direct comparison to a benchmark study. Figure 6 shows how the sorbent regeneration proceeded over temperature. The powder samples originated from the same batch of the spent sorbent for the tests of different ramp rates. The current work's maximum values of $d\alpha/dT$ were similar to the reported decarbonation under nitrogen (Table 2). The only deviation arose for the lowest heating rate of 2.5 °C/min. Compared to the thermally carbonated CaO that is initially synthesized using calcium nitrate and

citric acid, the mechanically carbonated CaO in this work had a higher regeneration rate at 2.5 °C/min heating rate. With higher heating rates, the maximum dα/dT values converged for thermally carbonated CaO and mechanically carbonated CaO, as expected.

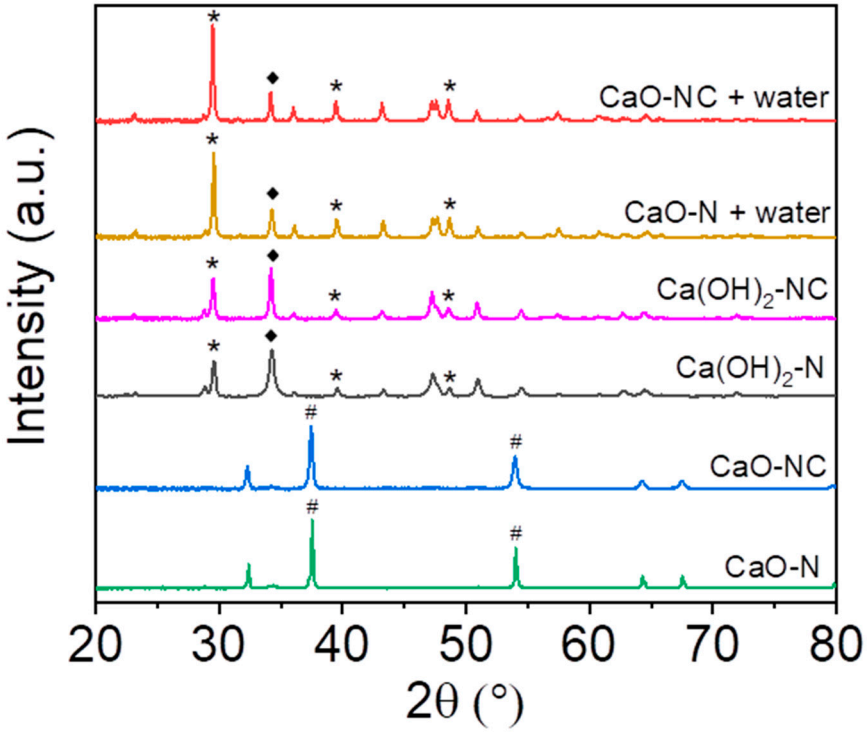

Figure 4. XRD patterns of carbonated sorbents. "*", " ♦ ", and "#" symbols represent $CaCO_3$, $Ca(OH)_2$, and CaO peaks, respectively.

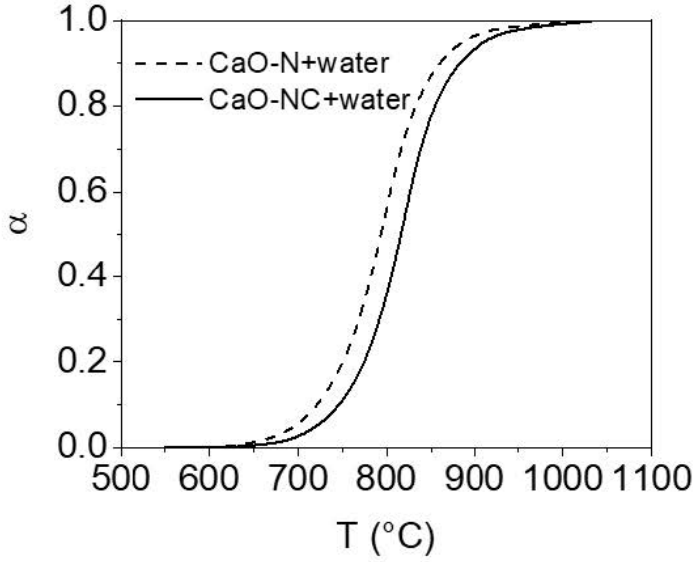

	CaO-N + water	CaO-NC + water
$d\alpha/dT$	0.011	0.013
α	0.55	0.53
T(°C)	799	818

Figure 5. Temperature-programmed sorbent regeneration curves for the two CaO sorbents milled with water. Heating rate: 10 °C. Values of maximum dα/dT, α, and temperature at the maximum dα/dT.

From the Friedman method, we can extract the effective activation energy for $CaCO_3$ decarbonation from the isoconversion temperatures and corresponding dα/dt values (Figure 7). Fedunik-Hofman et al. have found the effective activation energy E_α ranging from 171 kJ/mol to 147 kJ/mol within the conversion window of 0.1~0.9 [35]. The effective activation energy did not change much until 80% conversion. A certain decrease in E_α was

detected at conversion levels higher than 80% [35]. However, we have found a drastically different effective activation energy behavior for our mechanically carbonated sample. The effective activation energy was lower throughout the various conversion levels, and the magnitude started to decrease significantly from 50% conversion. It has been suggested that the change in the effective activation energy may come from the sample morphology evolution [35]. We can infer that our $CaCO_3$ will undergo a more drastic morphology change since it is prepared at nominal room temperature by reactive milling under CO_2 rather than typical carbonation at elevated temperatures. We do not think that the nature of the decarbonation gas (air vs. nitrogen) causes the observed effective activation energy behavior, since oxygen does not participate in the decarbonation reaction.

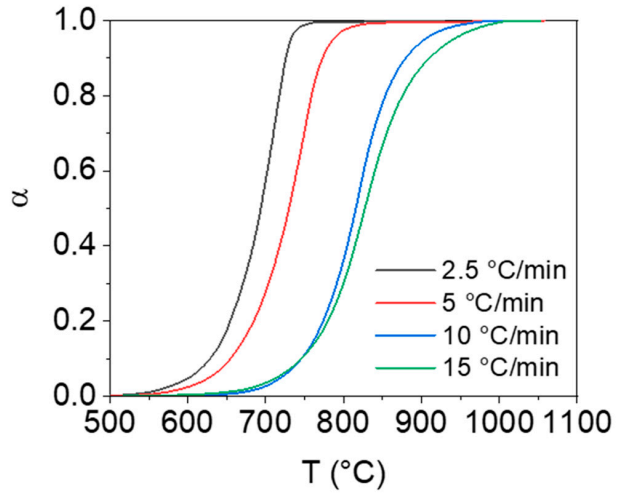

Figure 6. Sorbent regeneration curves for the spent "CaO-NC + water" sample.

Table 2. Maximum dα/dT value comparison for the "CaO-NC + water" sample decarbonation in air and $CaCO_3$ decarbonation in nitrogen.

Heating Rate (°C/min)	2.5	5	10	15
Air (this work)	0.033	0.016	0.013	0.0084
Nitrogen [35]	0.023	0.015	0.011	0.0086

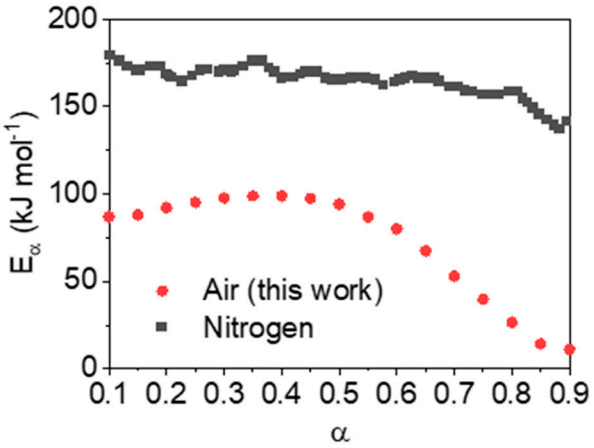

	This work	Fedunik-Hofman et al.
E_α (kJ mol^{-1})	11–99	147–171
Average E_α (kJ mol^{-1})	72	164

Figure 7. Effective activation energy E_α vs. α for the spent "CaO-NC + water" sample decarbonation in air and a reference $CaCO_3$ sample decarbonation in nitrogen. The nitrogen data points are from Fedunik-Hofman 2019.

4. Conclusions

We investigated the mechanically driven carbonation of calcium-containing sorbents at nominal room temperature. Two different CaO sorbents from calcium nitrate were synthesized: one with citric acid (high surface area, CaO-NC) and another without citric acid (low surface area, CaO-N). Calcium hydroxide sorbents were derived from these CaO sorbents.

Reactive milling carbonation was successfully conducted for 3 h in a milling jar filled with zirconia balls and 34.8 psia CO_2. For CaO sorbents, the higher surface area samples showed a higher consumption of CO_2; however, the conversion of the CO_2 was only around 40%. Since it is known that calcium hydroxides can quickly be carbonated, $Ca(OH)_2$ samples were milled under CO_2 to see if it is possible to achieve higher carbonation levels. We obtained a higher degree of carbonation; however, an unexpected CO_2 consumption plateau appeared for $Ca(OH)_2$-NC, the hydroxide sample with a higher surface area and corresponding higher initial carbonation kinetics. The wet agglomeration of the $Ca(OH)_2$-$CaCO_3$ composite, induced by byproduct water, complicated the mechanically driven carbonation process.

The most effective strategy was to add water to the CaO sorbents. The amount of water in this work (2.19 g H_2O per 2.27 g CaO) is notably different from the aqueous mineral carbonation processes. The in situ formation of the $Ca(OH)_2$ particles facilitated $CaCO_3$ formation during reactive milling. Interestingly, we saw crystalline $CaCO_3$ only when $Ca(OH)_2$ was involved in the reactive milling carbonation.

The effective activation energy extracted from temperature-programmed decarbonation tests showed a noticeable change against the sorbent regeneration level, deviating from the reported behavior of thermally carbonated CaO. Our mechanically carbonated sorbent undergoes more drastic morphology changes during decarbonation than thermally carbonated sorbents.

Supplementary Materials: The following supporting information can be downloaded at: https://www.mdpi.com/article/10.3390/inorganics11050200/s1, Figure S1: Pore diameter distributions of (a) CaO sorbents and (b) $Ca(OH)_2$ sorbents.; Figure S2: Nitrogen adsorption isotherms of (a) CaO sorbents and (b) $Ca(OH)_2$ sorbents.; Figure S3: Friedman analysis.

Author Contributions: Conceptualization, T.-S.O. and E.H.; methodology, S.M.T.K. and F.F.-K.-N.; formal analysis, S.M.T.K. and F.F.-K.-N.; resources, T.-S.O.; data curation, S.M.T.K.; writing—original draft preparation, S.M.T.K.; writing—review and editing, T.-S.O.; supervision, T.-S.O. All authors have read and agreed to the published version of the manuscript.

Funding: This research received no external funding.

Data Availability Statement: The data presented in this study are available on request from the corresponding author.

Conflicts of Interest: The authors declare no conflict of interest.

References

1. Grasa, G.S.; Abanades, J.C. CO_2 Capture Capacity of CaO in Long Series of Carbonation/Calcination Cycles. *Ind. Eng. Chem. Res.* **2006**, *45*, 8846–8851. [CrossRef]
2. Ridha, F.N.; Wu, Y.; Manovic, V.; Macchi, A.; Anthony, E.J. Enhanced CO_2 Capture by Biomass-Templated $Ca(OH)_2$-Based Pellets. *Chem. Eng. J.* **2015**, *274*, 69–75. [CrossRef]
3. Montes-Hernandez, G.; Chiriac, R.; Toche, F.; Renard, F. Gas–Solid Carbonation of $Ca(OH)_2$ and CaO Particles under Non-Isothermal and Isothermal Conditions by Using a Thermogravimetric Analyzer: Implications for CO_2 Capture. *Int. J. Greenh. Gas Control.* **2012**, *11*, 172–180. [CrossRef]
4. Kim, S.; Jeon, J.; Kim, M.-J. Vaterite Production and Particle Size and Shape Control Using Seawater as an Indirect Carbonation Solvent. *J. Environ. Chem. Eng.* **2022**, *10*, 107296. [CrossRef]
5. Criado, Y.A.; Arias, B.; Abanades, J.C. Effect of the Carbonation Temperature on the CO_2 Carrying Capacity of CaO. *Ind. Eng. Chem. Res.* **2018**, *57*, 12595–12599. [CrossRef]
6. Hanak, D.P.; Biliyok, C.; Anthony, E.J.; Manovic, V. Modelling and Comparison of Calcium Looping and Chemical Solvent Scrubbing Retrofits for CO_2 Capture from Coal-Fired Power Plant. *Int. J. Greenh. Gas Control.* **2015**, *42*, 226–236. [CrossRef]

7. Zhao, M.; Minett, A.I.; Harris, A.T. A Review of Techno-Economic Models for the Retrofitting of Conventional Pulverised-Coal Power Plants for Post-Combustion Capture (PCC) of CO_2. *Energy Environ. Sci.* **2013**, *6*, 25–40. [CrossRef]
8. Santos, M.P.S.; Manovic, V.; Hanak, D.P. Unlocking the Potential of Pulp and Paper Industry to Achieve Carbon-Negative Emissions via Calcium Looping Retrofit. *J. Clean. Prod.* **2021**, *280*, 124431. [CrossRef]
9. Hassani, E.; Feyzbar-Khalkhali-Nejad, F.; Rashti, A.; Oh, T.-S. Carbonation, Regeneration, and Cycle Stability of the Mechanically Activated $Ca(OH)_2$ Sorbents for CO_2 Capture: An In Situ X-Ray Diffraction Study. *Ind. Eng. Chem. Res.* **2020**, *59*, 11402–11411. [CrossRef]
10. Cazorla-Amoros, D.; Joly, J.P.; Linares-Solano, A.; Marcilla-Gomis, A.; Salinas-Martinez de Lecea, C. Carbon Dioxide-Calcium Oxide Surface and Bulk Reactions: Thermodynamic and Kinetic Approach. *J. Phys. Chem.* **1991**, *95*, 6611–6617. [CrossRef]
11. Lu, H.; Khan, A.; Pratsinis, S.E.; Smirniotis, P.G. Flame-Made Durable Doped-CaO Nanosorbents for CO_2 Capture. *Energy Fuels* **2009**, *23*, 1093–1100. [CrossRef]
12. Wang, J.; Huang, L.; Yang, R.; Zhang, Z.; Wu, J.; Gao, Y.; Wang, Q.; O'Hare, D.; Zhong, Z. Recent Advances in Solid Sorbents for CO_2 Capture and New Development Trends. *Energy Environ. Sci.* **2014**, *7*, 3478–3518. [CrossRef]
13. Hu, Y.; Liu, W.; Chen, H.; Zhou, Z.; Wang, W.; Sun, J.; Yang, X.; Li, X.; Xu, M. Screening of Inert Solid Supports for CaO-Based Sorbents for High Temperature CO_2 Capture. *Fuel* **2016**, *181*, 199–206. [CrossRef]
14. Hassani, E.; Cho, J.; Feyzbar-Khalkhali-Nejad, F.; Rashti, A.; Jang, S.S.; Oh, T.-S. Ca_2CuO_3: A High Temperature CO_2 Sorbent with Rapid Regeneration Kinetics. *J. Environ. Chem. Eng.* **2022**, *10*, 107334. [CrossRef]
15. Hassani, E.; Feyzbar-Khalkhali-Nejad, F.; Rashti, A.; Oh, T.-S. Solid-State Decomposition of Ca_2CuO_3 Enhances Its CO_2 Reactivity and Cycle Stability. *Fuel* **2023**, *332*, 126160. [CrossRef]
16. Sayyah, M.; Ito, B.R.; Rostam-Abadi, M.; Lu, Y.; Suslick, K.S. CaO-Based Sorbents for CO_2 Capture Prepared by Ultrasonic Spray Pyrolysis. *RSC Adv.* **2013**, *3*, 19872. [CrossRef]
17. Zhao, C.; Zhou, Z.; Cheng, Z. Sol–Gel-Derived Synthetic CaO-Based CO_2 Sorbents Incorporated with Different Inert Materials. *Ind. Eng. Chem. Res.* **2014**, *53*, 14065–14074. [CrossRef]
18. Martavaltzi, C.S.; Lemonidou, A.A. Parametric Study of the $CaO-Ca_{12}Al_{14}O_{33}$ Synthesis with Respect to High CO_2 Sorption Capacity and Stability on Multicycle Operation. *Ind. Eng. Chem. Res.* **2008**, *47*, 9537–9543. [CrossRef]
19. Li, Z.; Cai, N.; Huang, Y.; Han, H. Synthesis, Experimental Studies, and Analysis of a New Calcium-Based Carbon Dioxide Absorbent. *Energy Fuels* **2005**, *19*, 1447–1452. [CrossRef]
20. Yoon, H.J.; Lee, K.B. Introduction of Chemically Bonded Zirconium Oxide in CaO-Based High-Temperature CO_2 Sorbents for Enhanced Cyclic Sorption. *Chem. Eng. J.* **2019**, *355*, 850–857. [CrossRef]
21. Sultana, K.S.; Tran, D.T.; Walmsley, J.C.; Rønning, M.; Chen, D. CaO Nanoparticles Coated by ZrO_2 Layers for Enhanced CO_2 Capture Stability. *Ind. Eng. Chem. Res.* **2015**, *54*, 8929–8939. [CrossRef]
22. Ping, H.; Wu, S. CO_2 Sorption Durability of Zr-Modified Nano-CaO Sorbents with Cage-like Hollow Sphere Structure. *ACS Sustain. Chem. Eng.* **2016**, *4*, 2047–2055. [CrossRef]
23. Naeem, M.A.; Armutlulu, A.; Imtiaz, Q.; Donat, F.; Schäublin, R.; Kierzkowska, A.; Müller, C.R. Optimization of the Structural Characteristics of CaO and Its Effective Stabilization Yield High-Capacity CO_2 Sorbents. *Nat. Commun.* **2018**, *9*, 2408. [CrossRef]
24. Ramirez-Solis, S.; Dupont, V.; Milne, S.J. Preparation and Evaluation of CaO-Based CO_2 Sorbents Deposited on Saffil Fiber Supports. *Energy Fuels* **2018**, *32*, 8631–8640. [CrossRef]
25. Alshafei, F.H.; Minardi, L.T.; Rosales, D.; Chen, G.; Simonetti, D.A. Improved Sorption-Enhanced Steam Methane Reforming via Calcium Oxide–Based Sorbents with Targeted Morphology. *Energy Technol.* **2019**, *7*, 1800807. [CrossRef]
26. Liu, F.-Q.; Li, W.-H.; Liu, B.-C.; Li, R.-X. Synthesis, Characterization, and High Temperature CO_2 Capture of New CaO Based Hollow Sphere Sorbents. *J. Mater. Chem. A* **2013**, *1*, 8037. [CrossRef]
27. Broda, M.; Müller, C.R. Synthesis of Highly Efficient, Ca-Based, Al_2O_3-Stabilized, Carbon Gel-Templated CO_2 Sorbents. *Adv. Mater.* **2012**, *24*, 3059–3064. [CrossRef]
28. Ma, X.; Li, Y.; Yan, X.; Zhang, W.; Zhao, J.; Wang, Z. Preparation of a Morph-Genetic CaO-Based Sorbent Using Paper Fibre as a Biotemplate for Enhanced CO_2 Capture. *Chem. Eng. J.* **2019**, *361*, 235–244. [CrossRef]
29. Wei, S.; Han, R.; Su, Y.; Gao, J.; Zhao, G.; Qin, Y. Pore Structure Modified CaO-Based Sorbents with Different Sized Templates for CO_2 Capture. *Energy Fuels* **2019**, *33*, 5398–5407. [CrossRef]
30. Soong, Y.; Fauth, D.L.; Howard, B.H.; Jones, J.R.; Harrison, D.K.; Goodman, A.L.; Gray, M.L.; Frommell, E.A. CO_2 Sequestration with Brine Solution and Fly Ashes. *Energy Convers. Manag.* **2006**, *47*, 1676–1685. [CrossRef]
31. Montes-Hernandez, G.; Pérez-López, R.; Renard, F.; Nieto, J.M.; Charlet, L. Mineral Sequestration of CO_2 by Aqueous Carbonation of Coal Combustion Fly-Ash. *J. Hazard. Mater.* **2009**, *161*, 1347–1354. [CrossRef] [PubMed]
32. Gerdemann, S.J.; O'Connor, W.K.; Dahlin, D.C.; Penner, L.R.; Rush, H. Ex Situ Aqueous Mineral Carbonation. *Environ. Sci. Technol.* **2007**, *41*, 2587–2593. [CrossRef] [PubMed]
33. Porcheddu, A.; Cincotti, A.; Delogu, F. Kinetics of MgH_2 Formation by Ball Milling. *Int. J. Hydrog. Energy* **2021**, *46*, 967–973. [CrossRef]
34. Vyazovkin, S.; Burnham, A.K.; Criado, J.M.; Pérez-Maqueda, L.A.; Popescu, C.; Sbirrazzuoli, N. ICTAC Kinetics Committee Recommendations for Performing Kinetic Computations on Thermal Analysis Data. *Thermochim. Acta* **2011**, *520*, 1–19. [CrossRef]

35. Fedunik-Hofman, L.; Bayon, A.; Hinkley, J.; Lipiński, W.; Donne, S.W. Friedman Method Kinetic Analysis of CaO-Based Sorbent for High-Temperature Thermochemical Energy Storage. *Chem. Eng. Sci.* **2019**, *200*, 236–247. [CrossRef]
36. Hung, K.-C.; Yeh, H.; Yang, T.-C.; Wu, T.-L.; Xu, J.-W.; Wu, J.-H. Characterization of Wood-Plastic Composites Made with Different Lignocellulosic Materials That Vary in Their Morphology, Chemical Composition and Thermal Stability. *Polymers* **2017**, *9*, 726. [CrossRef] [PubMed]